

Experimental and theoretical investigation of fracture in glass matrix composites reinforced by alumina platelets

M.Kotoul, J. Pokluda & P. Šandera

Faculty of Mechanical Engineering, Brno University of Technology, Brno, Czech Republic

I. Dlouhý & Z. Chlup

Institute of Physics of Materials, Academy of the Czech Republic, Brno, Czech Republic

A. Boccaccini

Department of Materials, Imperial College London, London, United Kingdom

ABSTRACT: Experimental and theoretical investigation of fracture in the borosilicate glass/ Al_2O_3 platelets composite was performed. This composite is a perspective structural material for many applications due to its low production expenses and satisfactory properties even at elevated temperatures. The fractographical analysis was employed to reveal vitality of toughening mechanism with increasing content of reinforcement. Possible synergy between crack deflection and other toughening mechanisms was examined.

1 INTRODUCTION

Glass is known as a relatively cheap and easy to fabricate material with satisfactory properties. However, it is a material with very brittle behaviour (a typical fracture toughness value is around of $0.6 \text{ MPa.m}^{1/2}$). The low fracture toughness is a limiting factor for employing such material in design of loaded components. Therefore, an extensive research dedicated to the improvement of mechanical properties of inherently brittle materials including glass has taken place. There are many possible ways how to increase the fracture resistance. The possible synergy of more than one toughening mechanism is apparently advantageous. Particle/matrix interface decohesion and particle pull out, accompanied by deflection of crack trajectory provide the typical synergistic toughening effect.

A successful example of ceramic platelet reinforcement of glass is the borosilicate glass/ Al_2O_3 platelets composite developed by Boccaccini et al. (2003). They demonstrated a better mechanical behaviour of the composite over that of the unreinforced glass matrix in terms of hardness, Young's modulus, fracture strength and fracture toughness. By means of a detailed experimental investigation, the mechanical properties enhancement was ascribed to three concurrent phenomena: the Young's modulus increment resulting from the platelets addition, the presence of a compressive residual stress in the glassy matrix, and the crack deflection mechanism.

The paper aims to analyze a relationship between reinforcement volume fraction as well as surface roughness and mechanical properties especially frac-

ture toughness both experimentally and theoretically.

2 EXPERIMENTAL

The experimental glass ceramic composite was fabricated via powder technology and hot-pressing, as described in a previous study (Boccaccini & Trusty, 2003). Alumina platelets (TS100, Lonza-Werke, Waldshut-Tiengen, Germany) of hexagonal shape and with major axes between 5 and 25 μm and axial ratio of 0.2 were used. A commercially available borosilicate glass (DURAN, Shott Glass, Mainz, Germany) was selected for the composite matrix. Samples containing 0, 5, 10, 15 and 30 vol.% of platelets were considered in this study.

As was presented elsewhere (Boccaccini & Trusty, 2003, Tood et al., 1999) the composite microstructure exhibits a dense glass matrix where the platelets are distributed homogenously. The existence of a strong bond between the matrix and platelets was confirmed by transmission electron microscopy (Winn et al., 1997). The thermal expansion mismatch between matrix and reinforcement cause presence of internal residual stresses. The thermal expansion coefficient of the borosilicate glass matrix is much lower than that of the alumina platelets, which results in net tangential compressive and radial tensile stresses in the matrix upon cooling from the processing temperature. The measurement of these residual stresses was conducted by fluorescence spectroscopy technique, as reported in (Tood et al., 1999).

Fracture toughness values were obtained using the chevron notch technique. Test pieces of standard

cross-section ($3 \times 4\text{mm}$) were cut from the round shaped plates of diameter 40mm and thickness of 4mm by precise diamond saw. The chevron notch with top angle of 90° was machined by ultra thin diamond blade into each test piece. A Zwick/Roell electromechanical machine was used for loading in three point bend test with a span of 20mm . Cross-head speed of 0.1mm/min was used for loading. The samples were tested at room temperature and at 500°C . The elevated temperature has been selected just below the temperature of viscous flow of the glass matrix. The Maytec high temperature furnace was used to conduct tests at elevated temperatures. Load-deflection traces were recorded and the fracture toughness was calculated from the maximum load (F_{\max}) and the corresponding minimum value of geometrical compliance function (Y^*_{\min}) using the equation

$$K_{IC} = \frac{F_{\max}}{B\sqrt{W}} Y^*_{\min}, \quad (1)$$

where B and W stand for the width and height of the specimen, respectively. The calculation of the geometrical compliance function was based on Bluhm's slice model (Bluhm, 1975). Reliability of this technique for composite materials was reported elsewhere (Boccaccini et al., 2003, Dlouhy & Boccaccini, 2001).

Scanning electron microscopy (SEM) was used for fractographic analyses of fracture surfaces of tested chevron notched specimens.

Fracture surface roughness was measured by profilometer MicroProf FRT using a chromatic aberration method for z-axis measurement. The FRT Mark III software was applied for analysis of measured fractured surfaces and 3D surface reconstructions.

A plot of fracture toughness values on the volume content of alumina platelets in borosilicate glass matrix is shown in Figure 1.

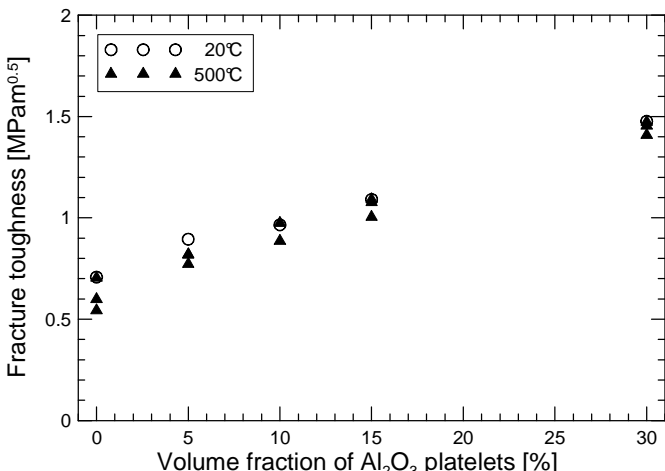


Figure 1. Dependence of fracture toughness on alumina platelets volume fraction in glass matrix at room and elevated temperature.

The combination of toughening mechanisms puts into effect during crack propagation which has an influence on fracture surface formation. Therefore the fracture surface characteristics indicate the employment of toughening mechanisms during different stages of fracture process. Figure 2 shows a dependence of relative surface roughness on alumina platelets content accompanied by fracture toughness data at room temperature. The surface roughness is linearly increasing with rising amount of alumina platelets in the borosilicate glass matrix up to approximately 15 vol. %. At higher reinforcement content the roughness increase is slowing down. Figure 2 compares the change of surface roughness and the evolution of fracture toughness with platelets volume fraction.

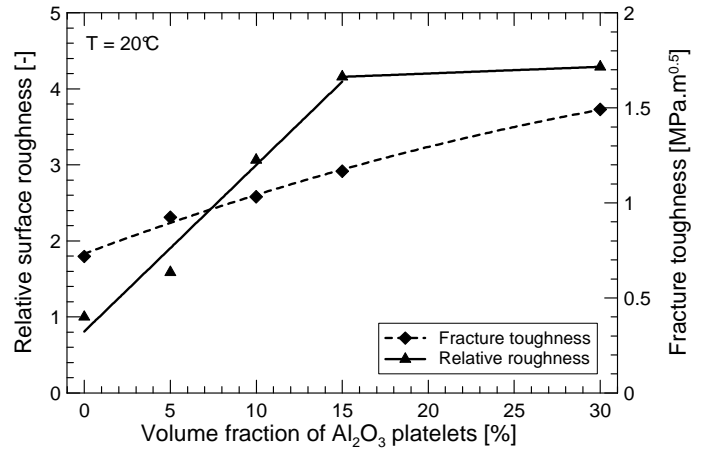


Figure 2. Dependence of relative surface roughness and fracture toughness on alumina platelets volume content in glass matrix at room temperature.

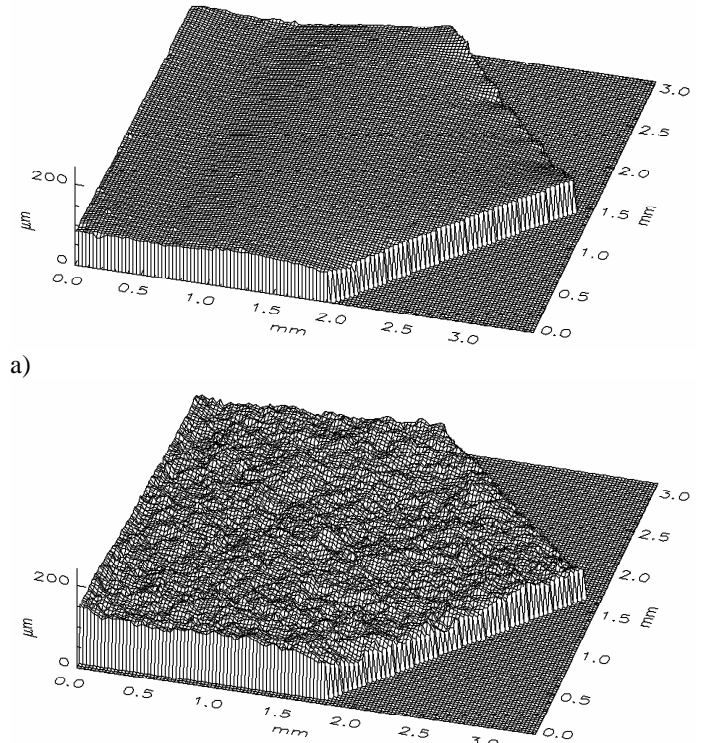
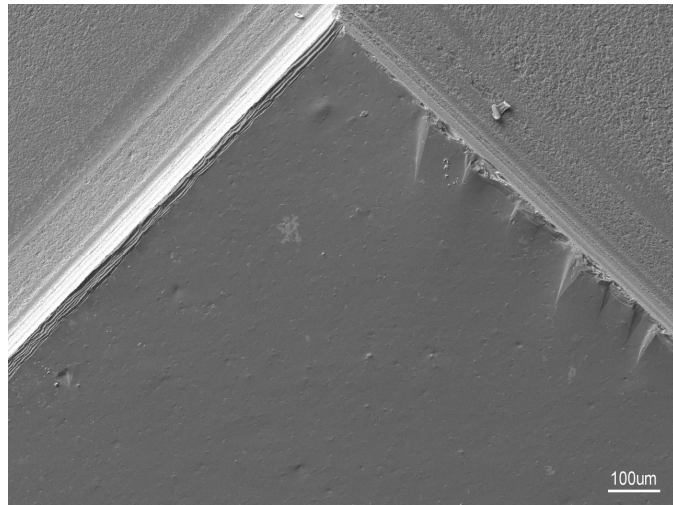
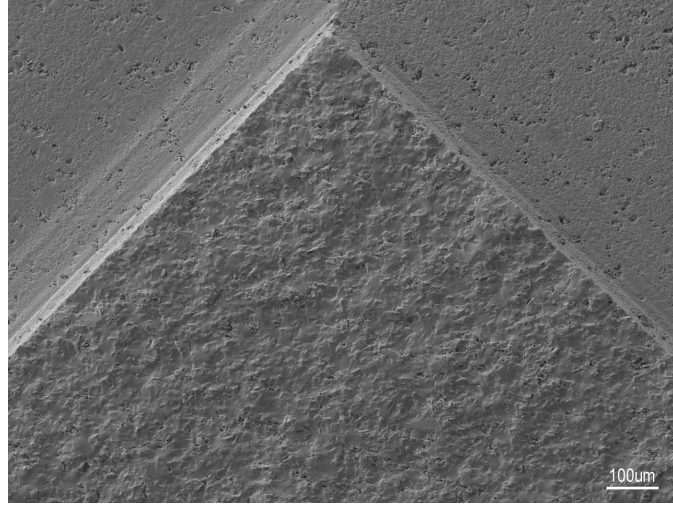


Figure 3. Reconstructed fracture surface for a) 0% and b) 30 % volume fraction of alumina platelets in borosilicate matrix.

The two main toughening mechanisms responsible for roughness (pull out and crack deflection) are weakened at the highest reinforcement volume fraction and therefore the increase of fracture toughness increase is lower in comparison to lower content of platelets. On the contrary, the higher content of alumina platelets, which are tougher than the glass matrix, is acting against the weakening of key toughening mechanisms. Typical examples of reconstructed fracture surface obtained from the profilometric measurement conducted on the fracture surfaces of chevron notch test pieces for both 0% and 30% of alumina platelets volume content in borosilicate glass matrix are shown in Figure 3. The corresponding scanning electron images are displayed in Figure 4. It is evident that the fracture surface roughness has been significantly increased when reinforcement is incorporated into the borosilicate glass. The connection between surface roughness and reinforcement volume content was proved however the roughness will certainly depend on the shape and dimension of the platelets as well as on the bonding between platelets and matrix.



a)



b)

Figure 4. Fracture surface for a) 0% and b) 30% volume content of alumina platelets in borosilicate glass matrix (SEM).

The fractographical analysis proved presence of several toughening mechanisms. The micrographs

supplying the evidence of examples of crack deflection and particle pull out are shown in Figure 5.

At the highest volume fraction of alumina platelets in borosilicate glass matrix, not all particles interacting with the crack front (present at the fracture surface) contribute to toughening effect as shown in Figure 6. Platelets cluster are observed even though a desirable degree of homogenous particles distribution is reached.

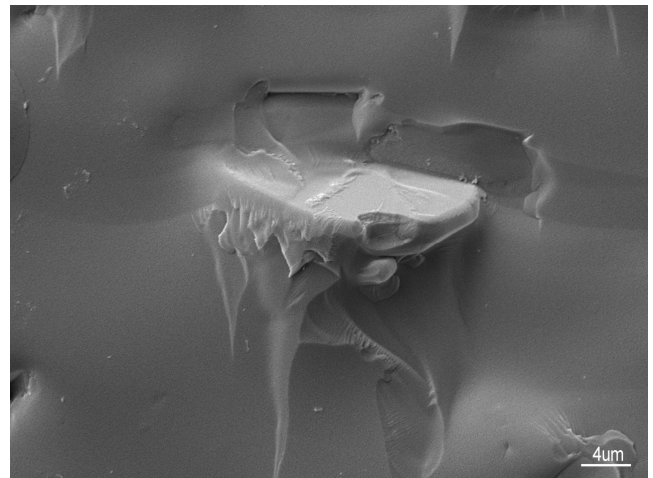
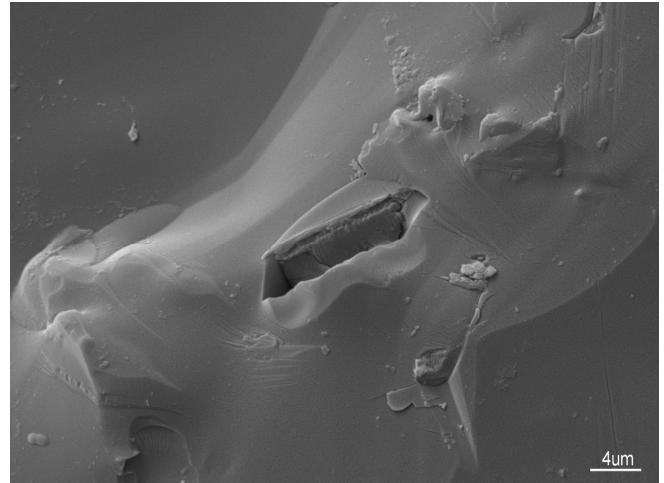


Figure 5. Example of toughening mechanisms evidence in the SEM image of fracture surface.

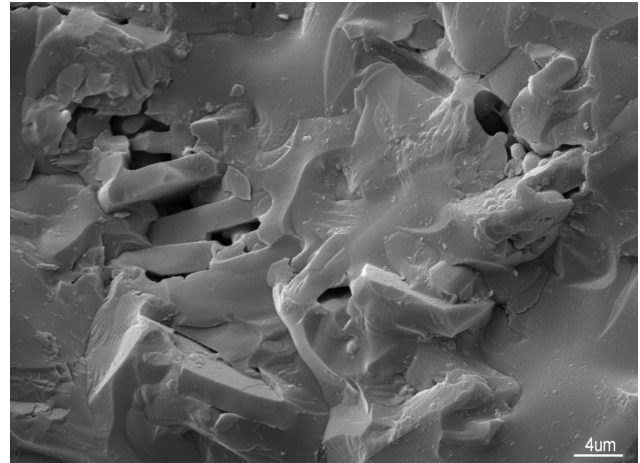


Figure 6. Clustering of alumina platelets when high reinforcement content is present.

3 THEORETICAL

The most comprehensive model for describing toughening by crack deflection has been developed by Faber & Evans (1983). This model uses a strain energy release rate approach where the ratio between the average strain energy release rate at the deflected crack front $\langle G \rangle$ and the strain energy release rate for the undeflected crack front G_{Im} gives the relative toughening. Crack advance is assumed to be governed by the strain energy release rate

$$G = \frac{1}{E} \left[k_1^2 (1-v^2) + k_2^2 (1-v^2) + k_3^2 (1+v) \right], \quad (2)$$

where k_1 , k_2 , and k_3 are the local stress intensities for the deflected segments along the crack front, and E and v are the Young modulus and Poisson's ratio, respectively. The toughening increment G_c is predicted as

$$G_c = \frac{G_{Im}}{\langle G \rangle} G_{Imc}, \quad (3)$$

where G_{Imc} stands for the critical energy release rate of the matrix. We have corrected some errors in the expression for the strain energy release rate derived by Faber & Evans, (1983) and obtained

$$\begin{aligned} \frac{G}{G_{Im}} = & \cos^2 \frac{\lambda}{2} \left(2v \sin^2 \phi + \cos^2 \frac{\lambda}{2} \right)^2 \cos^4 \phi + \cos^2 \phi \times \\ & \times \sin^2 \frac{\lambda}{2} \cos^4 \frac{\lambda}{2} + \frac{\cos^2 \frac{\lambda}{2} \sin^2 \phi \cos^2 \phi}{1-v} \left(2v - \cos^2 \frac{\lambda}{2} \right)^2, \end{aligned} \quad (4)$$

where λ is a tilt angle and ϕ is a twist angle. Observe that the expression in Equation 4 possesses the required limiting properties, i.e.

$$\lim_{\phi \rightarrow \pi/2} \frac{G}{G_{Im}} \rightarrow 0, \quad \lim_{\phi \rightarrow 0} \frac{G}{G_{Im}} \rightarrow \cos^4 \frac{\theta}{2}. \quad (5)$$

Faber and Evans considered cracks deflected by spheres, discs, and randomly oriented short rods (whiskers). In the case of disc shaped particles, there is necessary to describe the disc orientation with respect to the crack front and to adjacent discs. The effective tilt angle $\lambda \equiv \theta$ was introduced, and, by virtue of the particle geometry, the average tilt angle $\langle \lambda \rangle$ can be expressed as

$$\langle \lambda \rangle = \frac{\alpha/2 \theta_1 \sin \theta_1 + (1-\beta)/2 \theta_2 \sin \theta_2}{\alpha \sin \theta_1 + (1-\beta) \sin \theta_2}, \quad (6)$$

where the angles θ_1 and θ_2 describe the tilt of neighbouring discs with respect to the plane xz occupied by a planar crack, $\alpha, \beta \in \langle 0; 1 \rangle$ are relative locations at which the crack plane intercepts the discs. The twist angle ϕ of the crack between two adjacent discs is

$$\phi = \arctan \left[\frac{\alpha \sin \theta_1 + (1-\beta) \sin \theta_2}{\Delta'} \right], \quad (7)$$

where

$$\begin{aligned} \Delta' = & \left\{ \left[\frac{\Delta}{2r} - \alpha \cos \theta_1 \sin \mu_1 + (1-\beta) \cos \theta_2 \sin \mu_2 \right]^2 + \right. \\ & \left. + [\alpha \cos \theta_1 \cos \mu_1 + (1-\beta) \cos \theta_2 \cos \mu_2]^2 \right\}^{1/2}, \end{aligned} \quad (8)$$

where μ_1 and μ_2 are angles by which discs are offset with respect to the direction of crack propagation (parallel to the x -axis), Δ is the interparticle distance, approximated by the point-to-point spacing through the volume

$$\langle \Delta \rangle \sim N_v^{-1/3}, \quad (9)$$

where N_v is the number of particles per unit volume. Replacing λ by $\langle \lambda \rangle$ in Equation 4 and integrating over all possible configurations, the strain energy release rate due to twist of the crack front can then be written as

$$\begin{aligned} \frac{\langle G \rangle^t}{G_{Im}} = & \frac{4}{\pi^4} \int_{-\frac{\pi}{2}}^{\frac{\pi}{2}} \int_{-\frac{\pi}{2}}^{\frac{\pi}{2}} \int_0^1 \int_0^1 \int_0^{\frac{\pi}{2}} \int_0^{\frac{\pi}{2}} d\theta_1 d\theta_2 d\alpha d\beta d\mu_1 d\mu_2 \times \\ & \times \frac{\eta}{2} \left\{ \cos^2 \frac{\langle \lambda \rangle}{2} \left(2v \sin^2 \phi + \cos^2 \frac{\langle \lambda \rangle}{2} \right)^2 \cos^4 \phi + \right. \\ & + \cos^2 \phi \times \sin^2 \frac{\langle \lambda \rangle}{2} \cos^4 \frac{\langle \lambda \rangle}{2} + \\ & \left. + \frac{\cos^2 \frac{\langle \lambda \rangle}{2} \sin^2 \phi \cos^2 \phi}{1-v} \left(2v - \cos^2 \frac{\langle \lambda \rangle}{2} \right)^2 \right\}, \end{aligned} \quad (10)$$

where already the modification by the amount of crack front subject to twist was introduced via the factor η

$$\eta = \frac{\Delta}{2r} - \alpha \cos \theta_1 \sin \mu_1 + (1-\beta) \cos \theta_2 \sin \mu_2 \quad \sqrt{\Delta'^2 + [\alpha \sin \theta_1 + (1-\beta) \sin \theta_2]^2}. \quad (11)$$

η is the ratio of the undeflected to twisted crack front lengths.

For θ_1 and θ_2 of like-sign, the resultant tilted crack, occurring along one-half of the crack front has a driving force normalized with respect to the length of undeflected crack

$$\frac{\langle G \rangle^t}{G_{Im}} = \frac{4}{\pi^4} \int_{-\frac{\pi}{2}}^{\frac{\pi}{2}} \int_{-\frac{\pi}{2}}^{\frac{\pi}{2}} \int_0^1 \int_0^1 \int_0^{\frac{\pi}{2}} \int_0^{\frac{\pi}{2}} \frac{\xi}{2} \cos^4 \frac{\bar{\lambda}}{2} d\theta_1 d\theta_2 d\alpha d\beta d\mu_1 d\mu_2, \quad (12)$$

where ξ is the ratio of the undeflected to tilted crack front lengths

$$\xi = \frac{\Delta}{2r} - \alpha \cos \theta_1 \sin \mu_1 + (1-\beta) \cos \theta_2 \sin \mu_2 \quad (13)$$

$$\sqrt{\Delta'^2 + [\alpha \sin \theta_1 - (1-\beta) \sin \theta_2]^2}$$

and

$$\bar{\lambda} = \frac{1}{2} \left[\arctan \left(\frac{\tan \theta_1}{\cos \mu_1} \right) + \arctan \left(\frac{\tan \theta_2}{\cos \mu_2} \right) \right] \quad (14)$$

is the average tilt angle across the tilted plane.

The total strain energy release rate in the presence of discs is

$$\langle G \rangle = \langle G \rangle^t + \langle G \rangle^r. \quad (15)$$

The toughening increment derived from Equations 3 and 15 by numerical integration is plotted in Figure 7. Apparently, the crack deflection model fairly predicts the toughening increment up to the volume fraction of Al_2O_3 platelets about of 10 vol. %. However, for the volume fraction of 30 vol. % the deflection alone underestimates the experimental data by about of 50%.

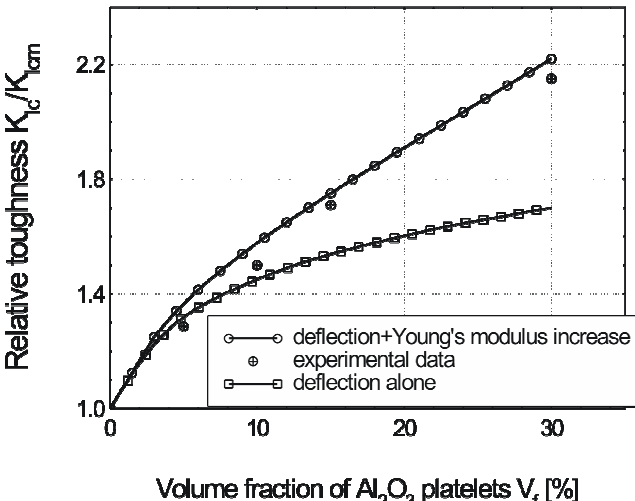


Figure 7. Relative toughness predictions base upon crack deflection model and upon the combination of the crack deflection+Young's modulus increase model.

Other toughening mechanism in this material could be considered: a contribution of residual stresses to toughening, an increase in fracture toughness due to the increase in Young's modulus resulting from the platelets additions (Table 2), and the crack trapping (Xu et al., (1998)). Note that no extensive crack bridging by Al_2O_3 platelets was observed.

Table 1. Thermomechanical properties of the composite constituents

	E [GPa]	G [GPa]	v	α [$10^{-6}/^\circ\text{C}$]
Glass matrix	63	26	0.22	3.3
Al_2O_3 platelets	402	248	0.23	8.9

One of several possible events may occur whenever the crack meets the particles. If the particle toughness exceeds that of the matrix, and the particles are strongly bonded to the surrounding material, then the crack is trapped by the particles. This process can significantly improve the strength of a brittle solid. However, for trapping to be effective, the particle toughness must be at least three times that of the matrix. If the particles have a low toughness, the crack breaks through them, and the toughness of the composite is little better than that of the matrix. Observe that for the composite investigated, the ratio of the particle fracture toughness K_{Ic}^{part} and the matrix fracture toughness K_{Icm} is about of 3.5. More generally, Bower & Ortiz, 1993 suggested that for bridging particles to form the particle critical strain energy release rate G_{Ic}^{part} should exceed

$$\frac{G_{Ic}^{part}}{G_{Imc}} \geq \left(2,1 + 4,8 \frac{R}{b} \right)^2, \quad (16)$$

where R denotes the particle radius and b is the particle spacing. If this is not the case, the crack cuts through the particles: the maximum possible toughness of the composite is then (Rose, 1975)

$$\frac{G_{Ic}^{eff}}{G_{Imc}} = 1 + 2 \frac{R}{b} \left(\frac{G_{Ic}^{part}}{G_{Imc}} - 1 \right). \quad (17)$$

If G_{Ic}^{part} is comparable to G_{Imc} , very little improvement in toughness is observed. This is the case of the composite investigated due to a high difference of Young's modulus, see Table 1.

Table 2. Young's modulus of borosilicate glass containing Al_2O_3 platelets

Platelet content [%]	E [GPa]
0	63
5	65
10	70
15	79
30	102

In the case that $\alpha_f > \alpha_m$ (where α_f and α_m are the coefficients of thermal expansion of the second phase and matrix, respectively), compressive hoop stresses and tensile radial stresses will exist around the second phase, and the crack (growing perpendicular to trajectories of maximum tensile stress) will deflect around the particle.

It was predicted (Tood et al., 1999) that the existence of local compressive stresses between the particles would decrease the stress intensity factor and hence contribute to toughening. However, in the direction normal to the disc-shaped inclusion, there is no constraint and the residual thermal tractions are very low in both the matrix and the inclusion. Thus, the crack prefers to deflect along the platelet inter-

faces while the twisted crack front between platelets is shortened due to a decrease of twist angle leading to higher energy release rate. As a result, both terms in Equation 3, G_{Imc} and $\langle G \rangle$ respectively, effectively increase and the net toughening increment does not change.

The effect of Young's modulus is easily to introduce using Equation 3. Namely, it holds

$$\frac{K_{Ic}}{K_{Imc}} = \sqrt{\frac{E}{E_m} \frac{G_c}{G_{Imc}}} = \sqrt{\frac{E}{E_m} \frac{G_{Imc}}{\langle G \rangle}}, \quad (18)$$

where E is Young's modulus of the composite, see Table 2. The toughening prediction based upon Equation 18 is plotted in Figure 7, too. It is seen that the agreement with experimental data is very good.

4 FRACTURE TOUGHNESS ASSESSMENT BASED UPON SURFACE ROUGHNESS ANALYSIS

For a sufficiently precise assessment of the roughness-induced shielding effect (RIS) the following steps must be undertaken:

- (i) Construction of a real-like model of the crack front based on a 3D determination of the surface roughness;
- (ii) Calculation of local stress intensity factors k_1 , k_2 and k_3 along the crack front;
- (iii) Calculation of the effective stress intensity factor K_{eff} .

The first step can be achieved by means of a 3D reconstruction of fracture morphology. This can be carried out by means of the MicroProf FRT based on the optical chromatography. The second problem can be solved using a numerical program system FRANC3D based on the boundary element method. The third step is solvable by a standard mathematics. The nearly exact numerical solution by means of the FRANC3D is, however, connected with extremely high time consumption, more or less inadequate to the efficiency of the results obtained. Therefore, a simple pyramidal model of the crack front was proposed (Pokluda et al., 2004) for approximate analytical estimations. This model is based on a pyramid-like periodical approximation of the tortuous crack front, which is characterized by respective tilt and twist angles Φ and Θ_m towards the macroscopic crack plane, see Figure 8. The profile roughness R_L (measured along the crack front) and the periodicity λ_{pl} (λ_{pp}) measured parallel (perpendicular) to the crack front are associated with the angles Φ and Θ_m (the highest twist angle of the pyramidal band) by following simple equations:

$$\lambda_{pp} \tan \Theta_m = \lambda_{pl} \tan \Phi, R_L = \cos^{-1} \Phi. \quad (19)$$

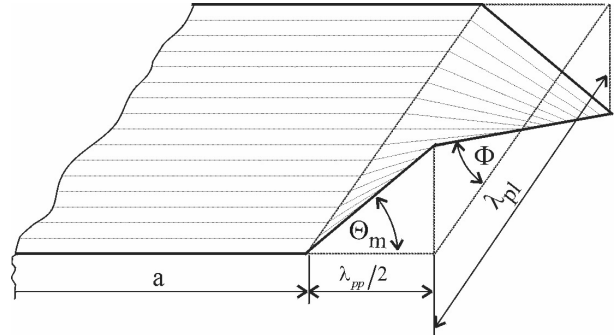


Figure. 8. Scheme of the pyramidal element periodically approximating the tortuous crack front.

The characteristic periodicities λ_{pp} and λ_{pl} are usually determined by Fourier analysis of the roughness profiles measured at appropriate locations on the fracture surface. The effective stress intensity factor k_{eff} for the pyramidal front (normalized by the remote K_I factor) can be calculated using the following approximate analytical expressions for local stress intensity factors:

$$\begin{aligned} k_1 &= \cos\left(\frac{\Theta}{2}\right) \left[2\nu \sin^2 \Phi + \cos^2\left(\frac{\Theta}{2}\right) \cos^2 \Phi \right], \\ k_2 &= \sin\left(\frac{\Theta}{2}\right) \cos^2\left(\frac{\Theta}{2}\right), \\ k_3 &= \cos\left(\frac{\Theta}{2}\right) \sin \Phi \cos \Phi \left[2\nu - \cos^2\left(\frac{\Theta}{2}\right) \right]. \end{aligned} \quad (20)$$

The results calculated according to Equation 20 are sufficiently accurate provided that $\lambda_{pp} \ll 2a$, where a is the precrack length. The global normalized effective factor k_{eff} for the pyramidal model of the crack front can then be computed as

$$k_{\text{eff}}^2 = \frac{\pi - 2}{2\Theta_m(2R_L + \pi - 4)} \int_{-\Theta_m}^{\Theta_m} \left(k_1^2 + k_2^2 + \frac{k_3^2}{1-\nu} \right) d\Theta. \quad (21)$$

Comparison of results obtained by means of the pyramidal model and the FRANC3D code revealed that, in the whole range of both the surface roughness and the roughness periodicity typical for real surfaces, the difference lies within the error band of 10%, (Pokluda et al., 2004). Thus, the pyramidal model is used hereafter for the assessment of the contribution of RIS to fracture toughness in investigated materials.

4.1 Results and analysis

The measurements of 3D fracture surface morphology were performed by means of the MicroProf FRT. The obtained profiles were subjected to the Fourier analysis in order to determine the characteristic periodicities λ_{pp} and λ_{pl} and, simultaneously, the corresponding profile roughness R_L were established. The measured values for all specimens are displayed in Table 3. Note that the values of λ_{pp} are

an order lower than the double-length of the pre-crack ($2a = 4$ mm) which ensures a reasonable validity of the pyramidal model. Determined roughness characteristics were then used for computation of the normalized effective factor k_{eff} according to Equations 19, 20, and 21; the results are also shown in Table 3.

Table 3. Computed characteristics of the pyramidal model related to measured specimens.

Sample	$\text{Al}_2\text{O}_3[\%]$	R_L	$\lambda_{\text{pp}} [\mu\text{m}]$	$\lambda_{\text{pl}} [\mu\text{m}]$	θ_m	k_{eff}
E6	0	1.011	373	114	0.0455	0.983
C2	5	1.053	412	171	0.3178	0.924
S1	10	1.199	102	32	0.2040	0.763
D3	15	1.115	341	170	0.2410	0.719
B6	30	1.229	102	128	0.7311	0.714

The dependence of the reciprocal value of k_{eff} , i.e. of the ratio K_{Ic}/K_{Imc} (predicted relative fracture toughness ratio) on the volume fraction of Al_2O_3 platelets is shown in Figure 9. It is clear that the RIS effect raises the fracture toughness of about 40 %.

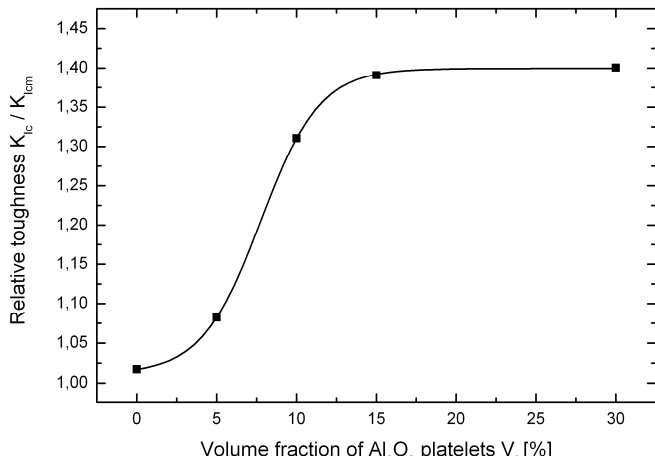


Figure 9. Influence of the roughness-induced shielding to fracture toughness as function of the percentage of Al_2O_3 particles

However, the saturation of the RIS effect starting at about 15 vol. % of Al_2O_3 is, most probably, associated with the resolution limit of the MicroProf FRT device. Namely, the angles of surface micro-facets higher than nearly 40% cannot be measured and, therefore, the roughness values are underestimated. The number of such facets rapidly increases for specimens with the content of Al_2O_3 platelets beyond 10 vol. %. Consequently, the real maximal contribution of the RIS effect to the enhancement of the fracture toughness can be, in fact, substantially higher than 50%. Observe that the theoretical prediction of the fracture toughness increment based upon Equation 3 is nearly 70%.

5 CONCLUSIONS

The fracture toughness values were determined at both room and elevated temperatures using the chevron

notch technique. The increase in fracture toughness values by incorporating 30 vol. % of alumina platelets into borosilicate glass matrix was of about $1.5 \text{ MPa}\cdot\text{m}^{0.5}$. This value is more than two times higher than the fracture toughness of plain borosilicate glass. Surface roughness of all fractured chevron notch test pieces was analysed with the aim to establish a relationship between the fracture resistance and the surface roughness. The surface roughness increases linearly up to 15 vol. % alumina platelets content in borosilicate glass matrix. This onset of roughness is followed by a steady state where changes in roughness are negligible. However, the analysis based upon the pyramid-like periodical approximation of the tortuous crack front (Pokluda et al., 2004) revealed that the saturation of the RIS effect starting at about 15 vol. % of Al_2O_3 is, most probably, associated with the resolution limit of the MicroProf FRT device. Theoretical calculations of the fracture toughness enhancement based upon corrected crack deflection model developed by Faber & Evans, (1983) combined with the influence of the increase in Young's modulus resulting from the platelets additions were found to be in good accordance with experimental data.

6 ACKNOWLEDGEMENT

The authors gratefully acknowledge financial support to Czech Science Foundation under project No. 106/06/0724.

REFERENCES

- Bluhm, J. I. 1975. Slice synthesis of a three dimensional “work of fracture” specimen. *Eng. Fract. Mech.* 7: 593-602.
- Boccaccini, A.R. & Trusty, P. A. 1996. Toughening and strengthening of glass by Al_2O_3 platelets, *J. Mat. Sci. Lett.* 15: 60-62.
- Boccaccini, A.R. & Winkler,V. 2002. Fracture surface roughness and toughness of Al_2O_3 platelet reinforced glass matrix composites. *Composites. Part A* 33:125-131.
- Boccaccini A.R. et al. 2003. Reliability of the chevron-notch technique for fracture toughness determination in glass. *Materials Science and Engineering A*347: 102-108.
- Bower, A.F. & Ortiz, M. 1993. The influence of grain size on the toughness of monolithic ceramic. *J. Engn. Mat. Technology* 115: 228-236.
- Breder, K. 2000. *Comprehensive Composite Materials* 4:77-93.
- Cannillo, V. et al. 2002. Numerical models for thermal residual stresses in Al_2O_3 platelets/borosilicate glass matrix composites. *Materials Science and Engineering A*323:246-250.
- Chou, Y. S. & Green, D.J. 1993. Silicon-carbide platelet alumina composites. 3. Toughening Mechanisms. *Am. Ceram. Soc. 76*: 1985-1992.
- Dlouhy I. & Boccaccini A. R. 2001. Reliability of the chevron notch technique for fracture toughness determination in glass composites reinforced by continuous fibres, *Scripta Mater.* 44: 531-537.

- Evans, A.G. & McMeeking, R. M. 1986. On the toughening of ceramics by strong reinforcements. *Acta met.* 34: 2435-2441.
- Faber, K.T.& Evans, A.G. 1983. Crack deflection processes—I. Theory. *Acta Met.* 31:565-576.
- Janssen, R. & Heussner, K.H. 1991. Platelet-reinforced ceramic composite materials, *Powder Metall. Int.* 23: 242-245.
- Huang, X. & Nicholson, P.S. 1993. Mechanical and fracture-toughness of α -Al₂O₃-platelet-reinforced Y-PSZ composites at room and high-temperatures. *J. Am. Ceram. Soc.* 76: 1294-1301.
- Pokluda, J. et al. 2004. Statistical approach to roughness-induced shielding effects. *Fatigue Fract. Engng. Mater. Struct.* 27: 1-17.
- Rawlings, R. D. 1994. Glass-ceramic matrix composites, *Composites* 25: 372-379.
- Rose, L.R.F. 1975. Toughening due to crack front interaction with a second phase dispersion. *Mechanics of Materials* 6: 11-15.
- Tood, R. I. et al. 1999. Thermal residual stresses and their toughening effect in Al₂O₃ platelet reinforced glass. *Acta Mat* 47: 3233-3240.
- Winn, A. J. et al. 1997. Examination of microhardness indentation-induced subsurface damage in alumina platelet reinforced borosilicate glass using confocal scanning laser microscopy. *J. Microscopy*, 186: 35-41.
- Xu, G. et al. 1998. The influence of crack trapping on the toughness of fiber reinforced composites. *J. Mech. Phys. Solids* 46: 1815-1833.